Journal of Alloys and Compounds 549 (2013) 324–335

Contents lists available at SciVerse ScienceDirect

Journal of Alloys and Compounds

journal homepage: www.elsevier.com/locate/jalcom

The effects of dendritic arm spacing (as-cast) and aging time (solution heat-treated) of Al–Cu alloy on hardness

B.P. Reis [a], R.P. França [a], J.A. Spim [b], A. Garcia [c], E.M. da Costa [a], C.A. Santos [a,*]

[a] Pontifical Catholic University of Rio Grande do Sul – PUCRS, Faculty of Engineering, Porto Alegre, RS, Brazil
[b] Federal University of Rio Grande do Sul – UFRGS, Department of Metallurgy, Foundry Laboratory, Porto Alegre, RS, Brazil
[c] University of Campinas – UNICAMP, Department of Materials Engineering, Campinas, SP, Brazil

ARTICLE INFO

Article history:
Received 13 July 2012
Received in revised form 7 September 2012
Accepted 10 September 2012
Available online 24 September 2012

Keywords:
Al–Cu alloy
Solidification
Secondary dendrite arm spacing
Solution heat treatment
Natural aging

ABSTRACT

The influences of dendritic arm spacing (as-cast condition) and aging times (solution treated condition) of a hypoeutectic Al–Cu alloy on hardness are analyzed in the present study. The solidification experiments were carried out at different conditions with respect to the cooling rate during solidification: cooled molds, and uncooled chill and sand molds. In any case, mold and metal were instrumented by thermocouples. Samples were extracted from all the castings and analyzed by optical microscopy in order to have the secondary dendrite arm spacing measured. These results were correlated with the solidification cooling rate and hardness. The samples were further subjected to solution heat treatment at a temperature of 540 °C for different solution times (8, 12, 16 and 28 h), followed by quenching in water at 25 °C. A solution time of about 12 h was shown to be the best condition for the solution heat treatment. After the solution heat treatment and during natural aging, the samples were analyzed by metallography and had their hardnesses measured. Experimental laws are proposed relating the resulting hardness to the aging time.

1. Introduction

Aluminum-based components are an important example for which the development of optimized microstructures during the solidification stage of processing can be fundamental for final properties and performance. It is well established that under most conditions of solidification, the dendritic morphology is the dominant characteristic of the microstructure of off-eutectic Al alloys. Fine dendritic microstructures in castings, characterized by the dendrite arm spacing, are recognized to affect mechanical and corrosion properties, yielding superior mechanical properties when compared with coarser ones, particularly when considering the tensile strength and ductility [1–10].

In order to improve the workability and keeping the strength, different heat treatments have been made mainly in wrought alloys. As is already well established, when Al–Cu cast alloys are subjected to the solution heat treatment, dissolution of the eutectic phase occurs, Cu is distributed in the α(Al-rich) matrix until saturation, when the $CuAl_2$ phase precipitates as fine particles within the matrix in the aging process, leading to improvements in mechanical properties. Various studies can be found in the literature including for wrought alloys of the series AA2xxx, AA6xxx and AA7xxx due to the higher response to hardening precipitation. The effect of solution temperature and time and cooling rate on the workability of the alloy AA2014 has been investigated by Gavgali and Aksakal [11], who analyzed the influence of different conditions such as temperature and time on the hot workability using hot tensile and torsion tests. Grazyna and Sieniawski have investigated the influence of the cooling rate after solution heat treatments on the microstructure and mechanical properties of AA6005 and AA6082 aluminum commercial alloys. The effect of the temperature of the solution treatment on the mechanism and kinetics of the aging process was analyzed by Brinell hardness measurements as a function of natural aging time in order to assess the effect of precipitation hardening [12]. For rheocast alloys some data are available in the literature such as those reported in the study developed by Zoqui and Robert [13], who analyzed structural modifications in rheocast Al–Cu alloys caused by heat treatment and the resulting implications on the mechanical properties. According to these authors, the coarse boundaries of $CuAl_2$ in the rheocast condition inhibit the growth of globules of the primary phase, being therefore responsible by the reduced growth rate. This condition is desirable in heat treatment practice; refined structures are generally associated with better mechanical properties than coarser ones. These authors claim that rheocast structures present advantages over dendritic microstructures. However, the literature is scarce on studies relating parameters of the as-cast dendritic

* Corresponding author. Tel.: +55 51 3353 7844; fax: +55 51 3353 4840.
E-mail address: carlos.santos@pucrs.br (C.A. Santos).

0925-8388/$ - see front matter © 2012 Elsevier B.V. All rights reserved.
http://dx.doi.org/10.1016/j.jallcom.2012.09.041

microstructure and heat treatment conditions, mainly solution and aging.

This work focuses on the influence of the scale of the dendrite arm spacing on the conditions of the solution heat treatment of a typical hypoeutectic as-cast Al–Cu alloy. The solidification experiments were performed utilizing both chill (cooled and uncooled) and sand molds instrumented by thermocouples, with the resulting samples being subjected to solution heat treatments at a constant temperature and different processing times.

2. Experimental procedure

In order to study the influence of the microstructure of an Al-4.0 wt.% Cu hypoeutectic alloy on the solution heat treatment time, a mother alloy was prepared in silicon carbide crucibles using a resistive furnace and commercially pure aluminum (99.6 wt.%) and electrolytic copper (99.8 wt.%). Table 1 shows the chemical composition of the alloy determined by Optical Emission Spectrometry (OES) corresponding to average values of five measurements in each sample, and the Al–Cu phase diagram [14].

2.1. Solidification conditions

2.1.1. Condition 1–unidirectional solidification

The casting assembly used in the experiments is shown in Fig. 1a. The main design criterion was to ensure a dominant unidirectional heat flow during solidification. This objective was achieved by adequate insulation of the chill casting chamber. An AISI 304 stainless steel chill was used, with the heat-extracting surface being polished. Experiments were performed using bottom cooling by compressed air [15]. Each alloy was melted until the molten metal reached a predetermined temperature. It was then stirred until the temperature was brought to a superheat of about 10% above the *liquidus* temperature. Temperatures in the chill and in the casting were monitored during solidification via the output of a bank of type K thermocouples (1.6 mm diameter) accurately located with respect to the metal/mold interface, as indicated in Fig. 1b. All the thermocouples were connected by coaxial cables to a data logger interfaced with a computer, and the temperature data were acquired automatically. Compressed air flow rates of 10, 20 and 30 L/min flow were used in the experiments. The system was previously calibrated using commercially pure aluminum, and the experiments were performed twice in order to have reproducibility assured.

2.1.2. Condition 2–non directional solidification

For these experiments, the alloys were melted in silicon carbide crucibles using a resistive furnace and poured into both: a rectangular sand mold (25 × 25 × 75 mm) and a cylindrical metallic mold (25 × 75 mm). A K-type thermocouple, located in the center of the mold cavity, was used to obtain the cooling curves during solidification [16]. In all the experiments the pouring temperature was kept at about 100 °C above the liquidus temperature. Fig. 2 presents a schematic representation of the experimental setup.

2.2. Metallography and dendrite arm spacing measurements

Traditional metallographic techniques were used for microstructure characterization: a 5% solution of hydrofluoric acid was used to etch the samples, followed by optical (OM) and scanning electron (SEM) microscopies. The chemical compositions of the phases and precipitates were determined by EDS (Energy Dispersive X-ray Spectroscopy). The secondary dendrite arm spacing (λ_2) was measured from the bottom to the top of the longitudinal section of the casting (Fig. 3a). About 20 measurements were taken for each position. The method was based on the mean distance among a number of adjacent secondary dendritic arms which are formed perpendicularly to the primary ramification and characterized by the following relationship [17]:

$$\lambda_2 = \frac{L}{n-1} \quad (1)$$

where L is the center to center distance of secondary ramifications and n is the adopted number of ramifications (Fig. 3b).

2.3. Solution heat treatment

Solution heat treatment experiments were carried out to analyze the dissolution of the copper-rich precipitate ($CuAl_2$) in the α-aluminum rich matrix as a function of λ_2. The samples, divided in groups, were heated at 540 °C into a resistive furnace (solution), and after that cooled in water at 25 °C (quench). The adopted nomenclature for the samples was:

- For unidirectional solidification: condition 1–1 – cooled using a 10 L/min air flow rate; condition 1–2 – cooled using a 20 L/min air flow rate; condition 1–3 – cooled using a 30 L/min air flow rate, with the solution time kept constant: 8 h;
- For non-directional solidification: condition 2–1 – solution time of 8 h; condition 2–2 – solution time of 12 h; condition 2–3 – solution time of 16 h; condition 2–4 – solution time of 28 h.

2.4. Hardness testing

Brinell hardness tests were performed with a 5 mm diameter tungsten ball and 2500 N (250 kg) load according to the ASTM E 10 – 04 standard [18]. The tests were carried out with samples in the as-cast condition, after solution heat treatment and during the natural aging. They correspond to average values of three measurements in each sample for each condition.

3. Results and discussion

3.1. First solidification condition

Figs. 4 and 5(a) and (b) show the typical cooling curves of conditions 1–1, 1–2 and 1–3, respectively. In the cooling curve of condition 1–1 (flow rate 10 L/min) the initial molten temperature was about 720 °C (average value between the first and last thermocouples) and the bottom mold temperature was about 625 °C. These figures also show the liquidus (TL = 645 °C) and non-equilibrium solidus (TS = 548 °C) temperatures for this alloy (dot horizontal lines). These values were determined by the inflections of the temperature curves and are in agreement with the corresponding phase diagram shown in Table 1. The cooling curves of condition 1–2 (flow rate 20 L/min) and condition 1–3 (flow rate 30 L/min) clearly display the decrease in local solidification time as a consequence of

Table 1
Chemical composition of the Al-4.0 wt.% Cu alloy [wt.%] and the Al–Cu phase diagram.

Composition (wt%)	
Al	Cu
95.57	4.04
Fe	Si
0.27	0.05
Mg	Others
0.01	0.06

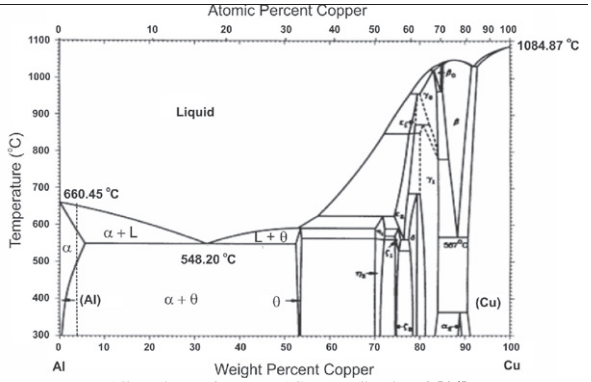

Alloy Phase Diagrams, ASM Handbook, v.3 **[14]**.

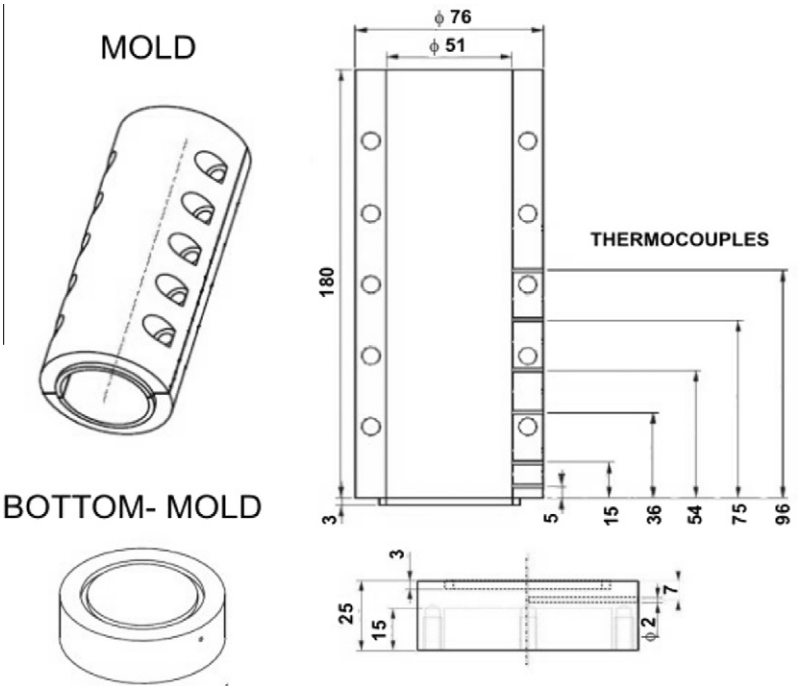

Fig. 1. Schematic representation of the first solidification condition, and details of the thermocouples positions.

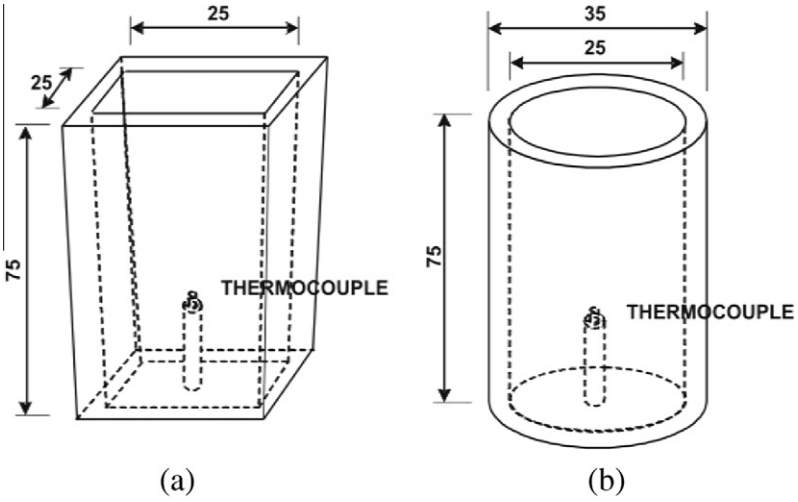

Fig. 2. Schematic representation of the second solidification condition: (a) sand mold, (b) metallic mold.

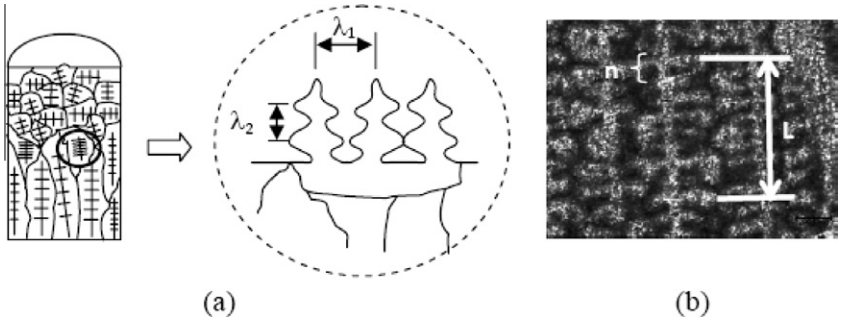

Fig. 3. Representation of the technique used to quantify the secondary dendrite arm spacing: (a) longitudinal section; (b) indication in a photomicrograph.

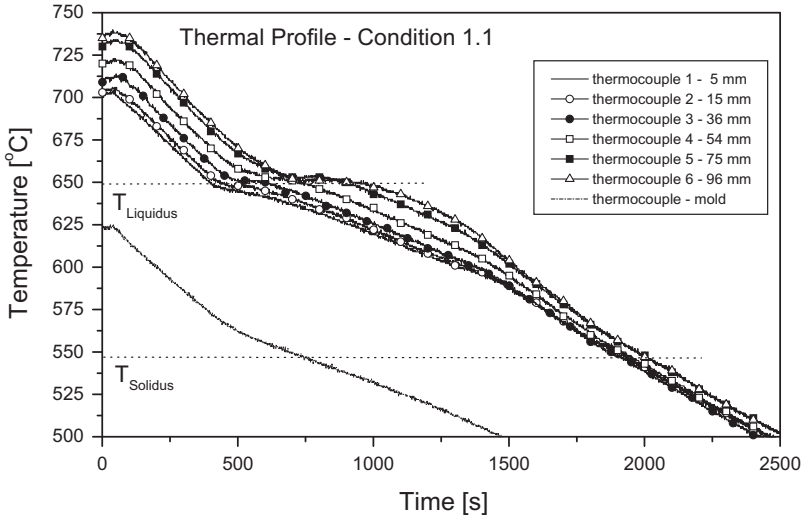

Fig. 4. Temperature curves measured by the thermocouples: condition 1.1 (10 L/min).

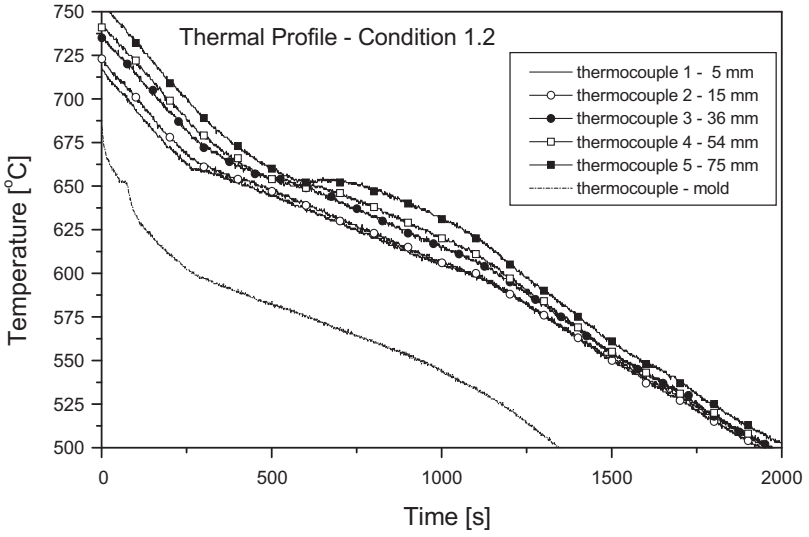

(a)

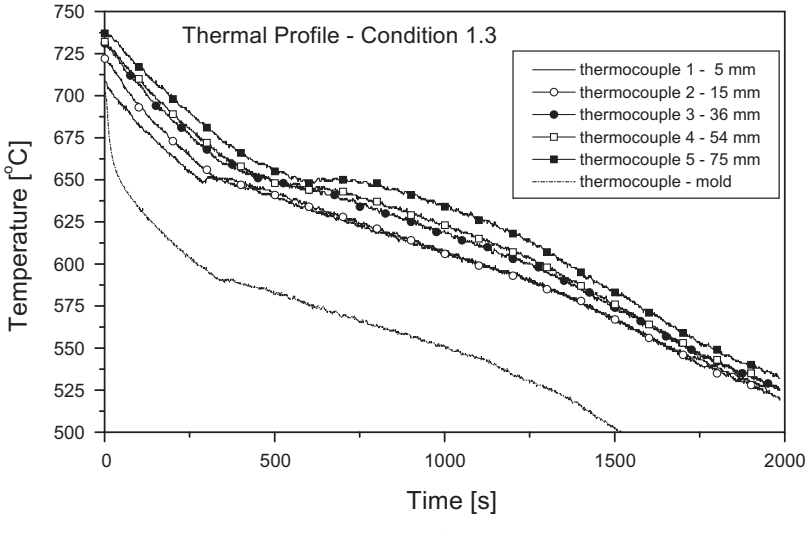

(b)

Fig. 5. Temperature curves measured by the thermocouples: (a) condition 1.2 (20 L/min), (b) condition 1.3 (30 L/min).

Table 2
Chemical composition along the casting length – Average values for all conditions.

Position	Element (wt.%)												
	Al	Cu	Fe	Mn	Mg	Zn	Ni	Cr	Pb	Sn	Ti	P	Si
1 (5 mm)	Bal.	4.17	0.40	0.22	0.09	0.093	0.10	0.079	0.04	0.040	0.029	0.012	0.05
2 (15 mm)	Bal.	4.13	0.15	0.04	0.01	0.005	0.03	0.024	0.01	0.013	0.005	0.001	0.01
3 (36 mm)	Bal.	3.98	0.04	0.01	0.01	0.005	0.01	0.005	0.01	0.010	0.005	0.001	0.01
4 (54 mm)	Bal.	3.95	0.16	0.04	0.01	0.005	0.02	0.014	0.01	0.014	0.005	0.001	0.01
5 (75 mm)	Bal.	3.95	0.04	0.02	0.01	0.011	0.01	0.005	0.01	0.010	0.005	0.001	0.01
6 (96 mm)	Bal.	3.93	0.01	0.02	0.01	0.005	0.01	0.005	0.01	0.010	0.005	0.001	0.01

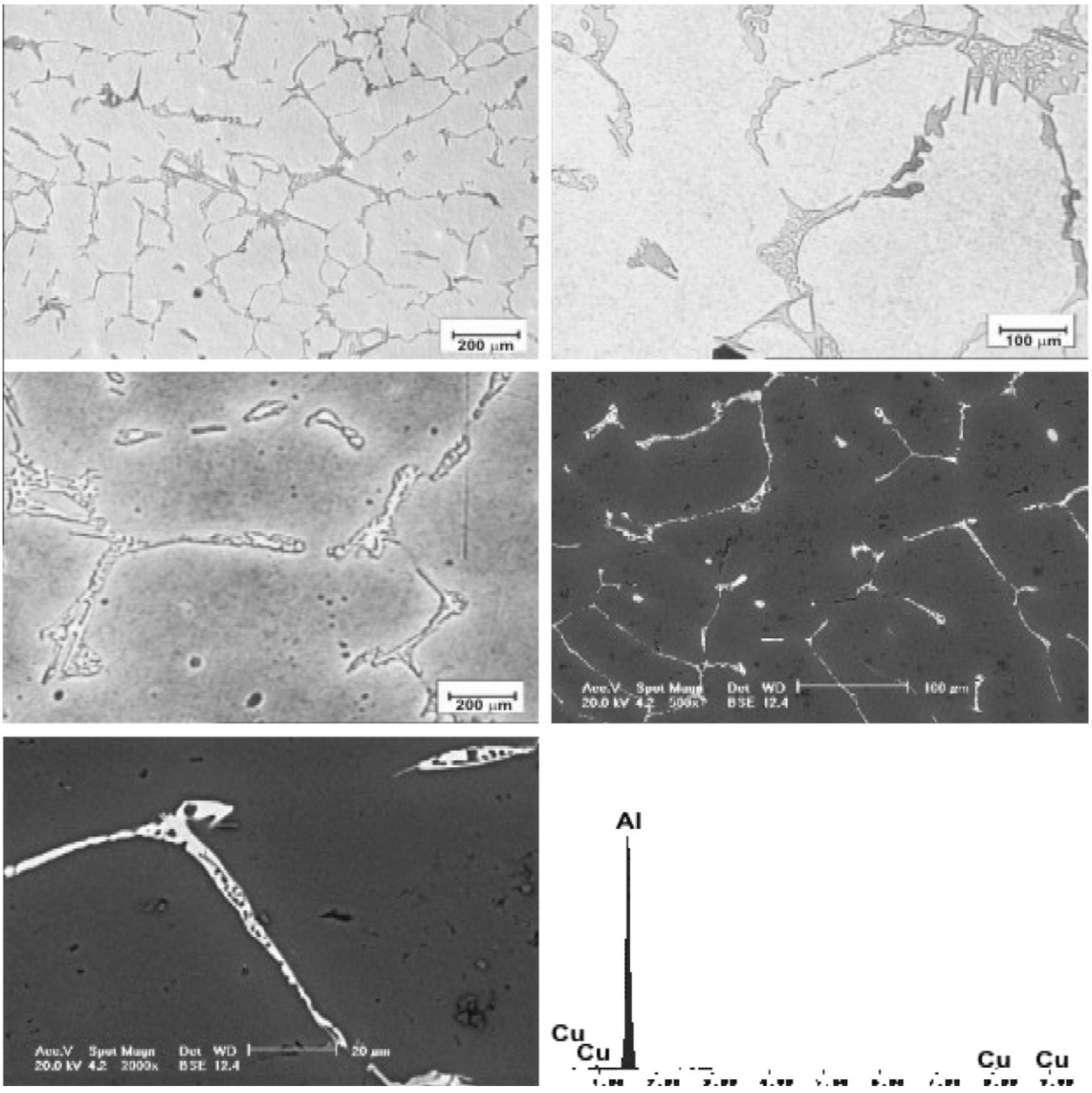

Fig. 6. Microstructures of transverse sections: condition 1–1. Positions 1 and 5.

the increase in cooling rate, (Fig. 5a, b). For the condition 1–2 the initial molten temperature was about 735 °C, the bottom mold temperature was about 680 °C and the temperature difference between the thermocouples was about 35 °C, while for the condition 1–3 the initial molten temperature was about 720 °C, the bottom mold temperature was about 700 °C and the temperature difference between the thermocouples was about 30 °C.

Transverse samples were analyzed by an Optical Emission Spectrophotometer (OES) for chemical composition, corresponding to 5 measurements for each position in casting (Table 2).

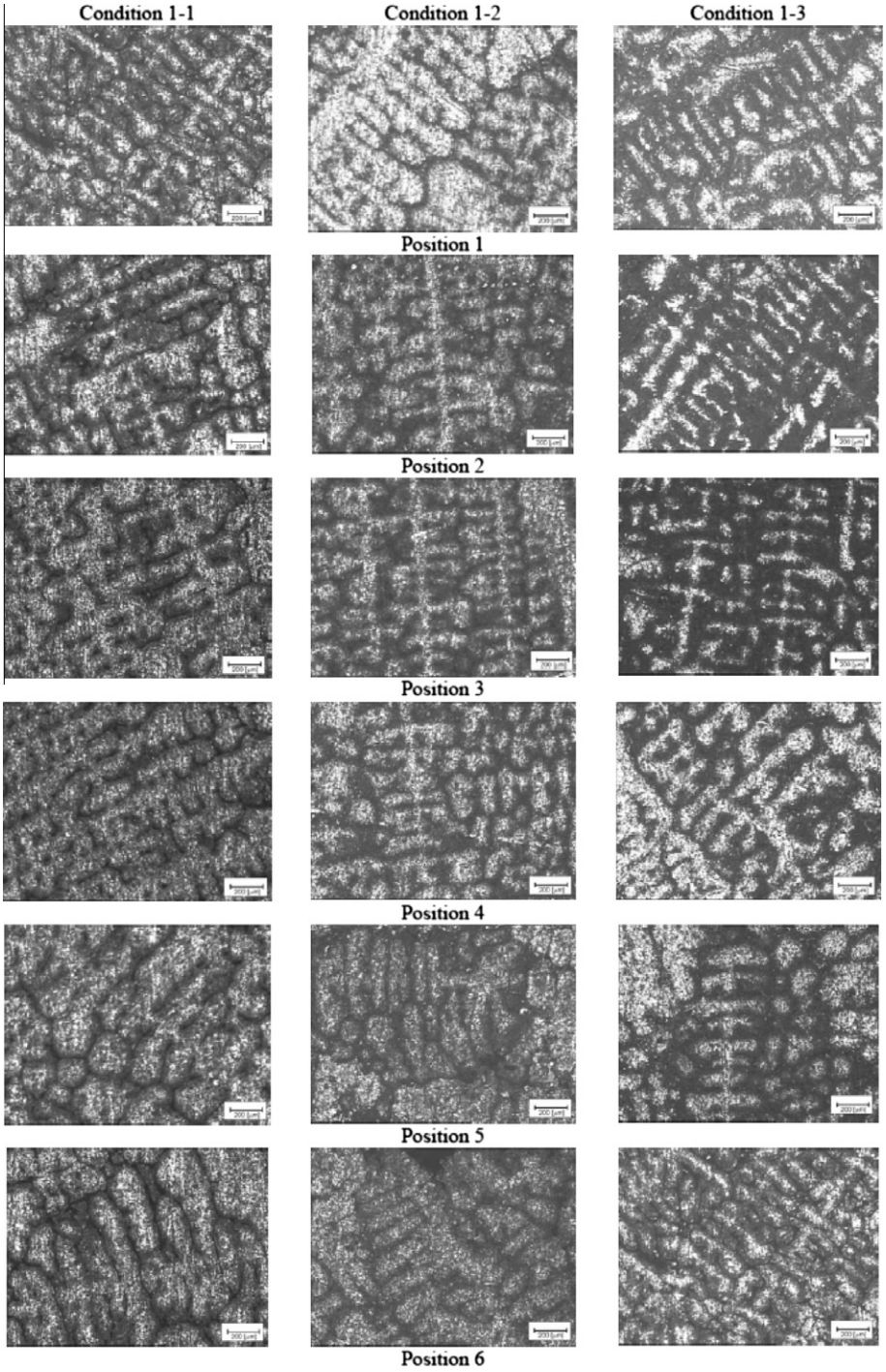

Fig. 7. Microstructures along the casting length depicting the dendritic structure. All conditions. Positions 1 to 6.

3.1.1. Solidification microstructures

Analyzing the microstructures along different transverse sections of condition 1–1, it can be observed an α–rich aluminum dendritic matrix and an interdendritic zone formed by a eutectic mixture of α and $CuAl_2$ intermetallic particles (Fig. 6). This microstructure is in accordance to the alloy phase diagram presented in Table 1 for the Al-4.0 wt.% Cu alloy. The samples were also analyzed by SEM (scanning electron microscope) coupled with EDS (Energy Dispersive X-ray Spectrometer) in order to certify the phases and precipitates.

In order to quantify the secondary dendrite arm spacing as a function of position along the longitudinal section of the castings (distance from metal/mold interface) about 20 to 25 measurements in each sample were carried out. No significant differences on the amount of precipitates along the range of solidification cooling rates examined were observed.

Fig. 7 depicts photomicrographs at different positions along the casting lengths. In the first position for all castings examined, the values of λ_2 are quite similar. After this position, λ_2 increases with the distance from the metal/mold interface.

The results of secondary dendrite arm spacing obtained in the various experiments are summarized in Fig. 8a, as a function of position along the castings length. These results appear consistent with the knowledge found in the literature relating microstructure

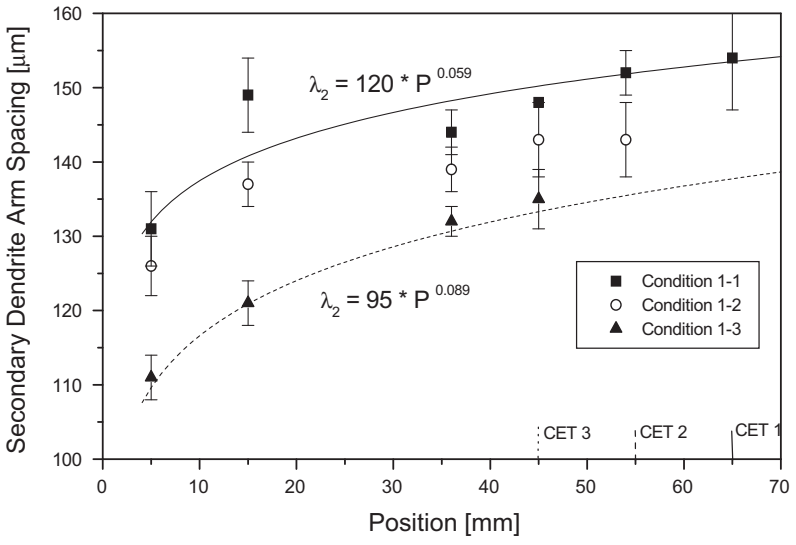

(a)

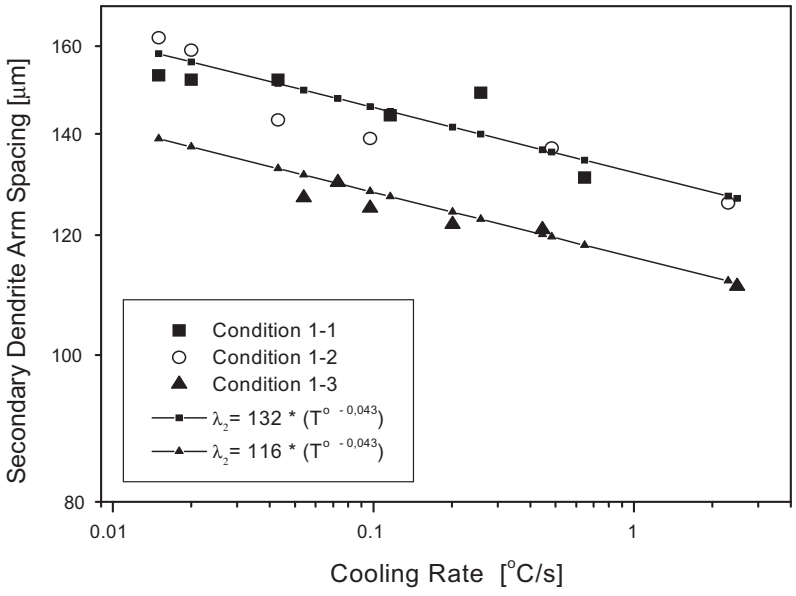

(b)

Fig. 8. (a) Secondary dendrite arm spacing as a function of position along the castings lengths; (b) as a function of the cooling rate.

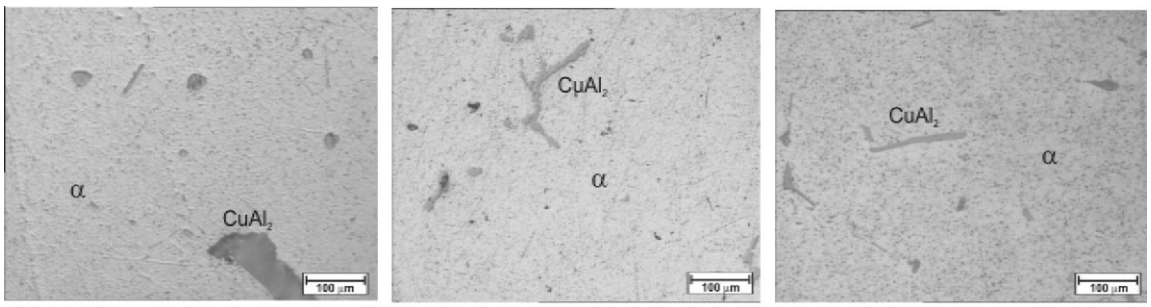

(a) (b) (c)

Fig. 9. Metallographic images of solution heat treated samples using 8 h: (a) condition 1–1, (b) condition 1–2, and (c) condition 1–3. Position 1 in all conditions.

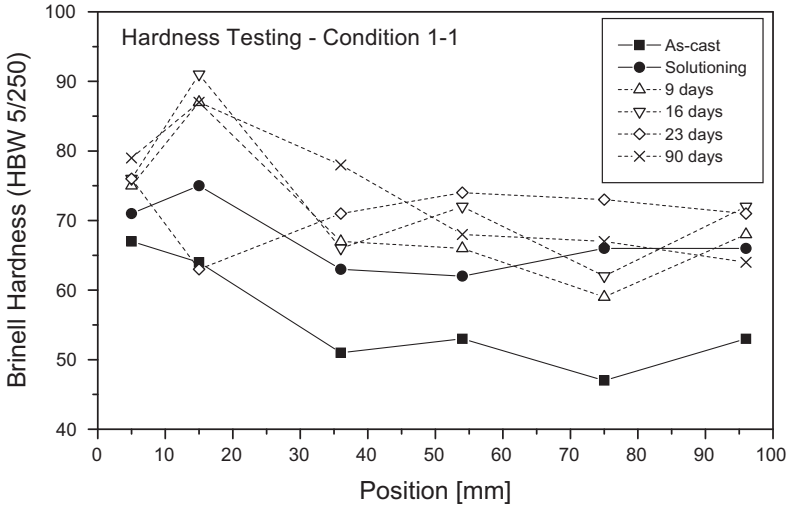

Fig. 10. Brinell hardness as a function of aging time and position in casting: – Condition 1–1.

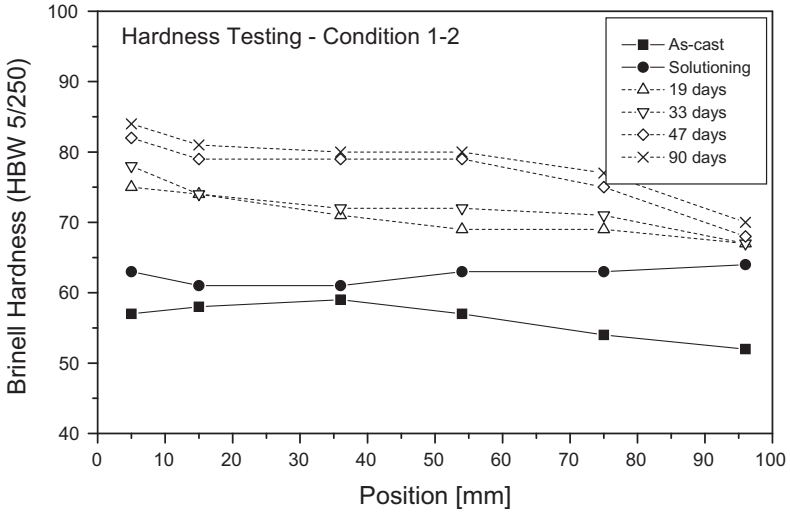

(a)

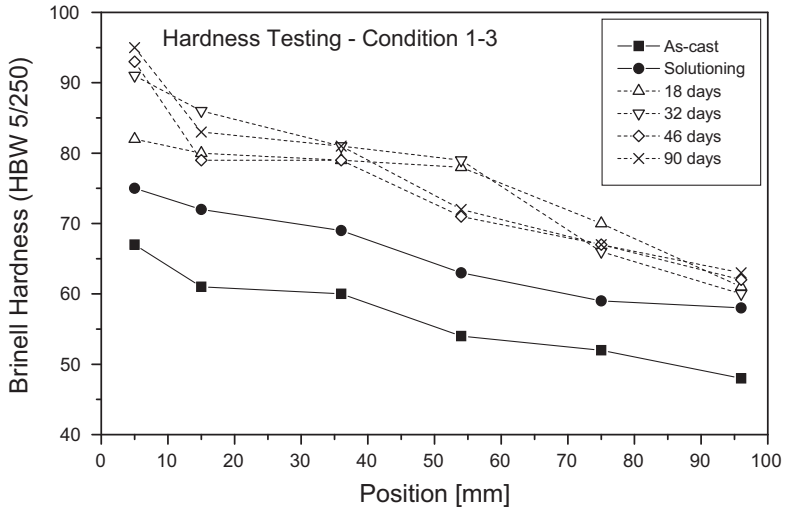

(b)

Fig. 11. Brinell hardness as a function of aging time and position in casting: (a) condition 1–2, (b) condition 1–3.

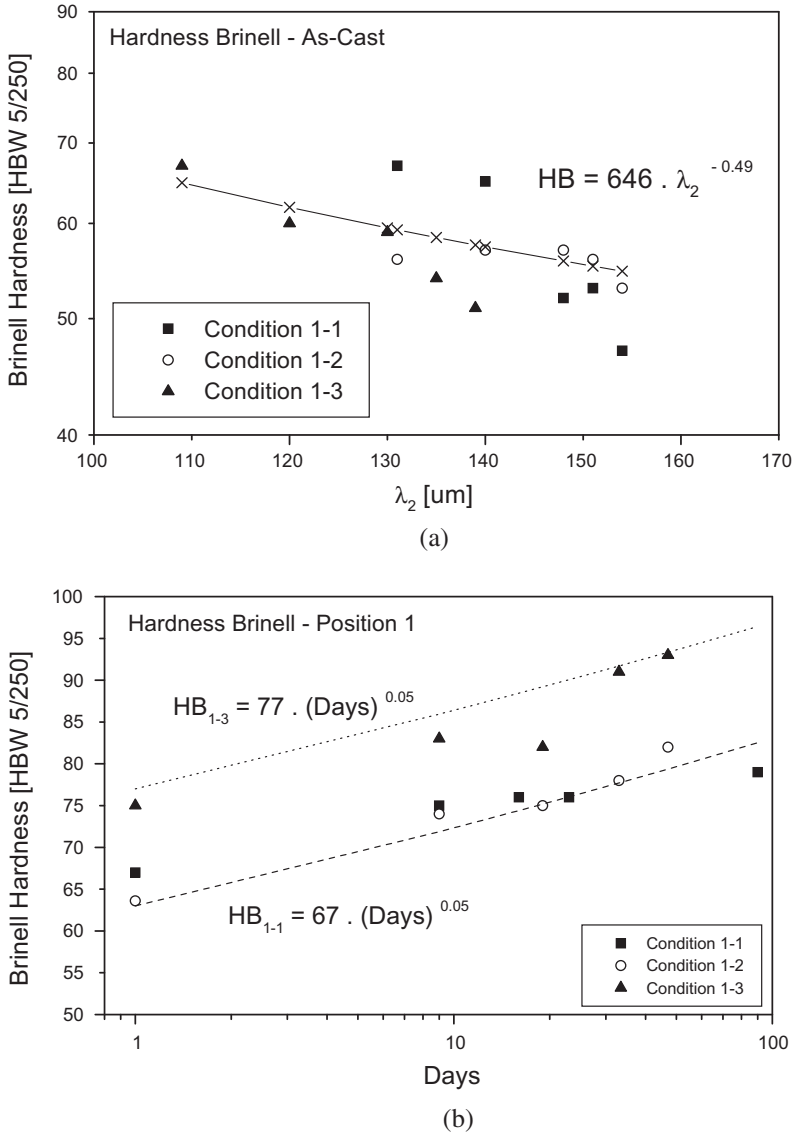

Fig. 12. Brinell hardness as a function of: (a) λ_2 in the as-cast condition, (b) aging time for position 1.

effects to solidification cooling rates [2,4,19,20]. The conditions 1–1 and 1–2 showed similar behaviors with higher values of dendrite arm spacings when compared with those of the condition 1–3. Fig. 8b presents a comparison between all conditions examined as a function of the cooling rate, which were experimentally determined by considering the thermal data recorded immediately after the passing of the liquidus isotherm by each thermocouple, as detailed in previous works [1,16].

3.1.2. Solution heat-treated microstructures

The solution treatment using 8 h resulted in dissolution of the Cu-rich phase. However, a small amount of this phase remained after the solution treatment, which decreased with the decrease in the secondary dendrite arm spacing (Fig. 9), and consequently with the increase in the air flow rate. This indicates that the increase in the cooling rate can result in a significantly lower volumetric fraction of CuAl2 (θ-phase) after the solution treatment. This occurs because the finer CuAl2 interdendritic phase is more easily dissolved than coarser interdendritic phase due to area/volume ratio. The grain growth during solution treatment was not examined in any case, since the focus was on the dendritic pattern inside the grains.

3.1.3. Hardness testing

The experimental results permitted a correlation between hardness, microstructure features, solution heat treatment and natural aging time to be established. For the condition 1–1 (Fig. 10) it is possible to observe a decrease in hardness along the casting length for the as-cast condition, with values between 65 HBW and 50 HBW. After the solution heat treatment, the hardness increased significantly for the all experimental conditions and during the natural aging time this increase was more moderate (70–80 HBW). The highest hardness was associated with position 2 (15 mm) probably due to lower occurrence of interdendritic microporosity. The high dispersion of measurements can be attributed to the slow cooling conditions during the experiments.

For conditions 1–2 and 1–3 the behavior of hardness was quite similar (Fig. 11). However, the highest values were generally associated with the 90 days aging period. The as-cast hardness clearly indicates that the solution treatment is necessary to permit better mechanical properties to be attained, as most of the strengthening alloying elements are not in solution. It can be seen that higher hardness is associated with smaller secondary dendritic arm spacings, i.e. with a more homogeneous distribution of the (θ) phase. This will permit a more efficient dissolution of the eutectic phase.

Table 3
Secondary dendrite arm spacing for sand mold and chill mold conditions.

Samples	λ_2 average (μm)	λ_2 minimum (μm)	λ_2 maximum (μm)
Sand mold	220	207	245
Chill mold	187	199	173

Fig. 12 shows the Brinell hardness as a function of λ_2 and aging time for all conditions. For the behavior of hardness with λ_2 for the as-cast condition (Fig. 12a), an equation has been fitted to the experimental scatter, which describes the decrease in hardness with the increase in λ_2 for all conditions. The results of hardness measured during natural aging (until 90 days) have also been fitted by equations permitting the hardness to be correlated with the aging time (Fig. 12b). The condition 1–3 (lower λ_2 and higher cooling rates) presented the highest hardness immediately after solution heat treatment, followed by conditions 1–2 and 1–1. Fig. 12b refers to position 1 (5 mm) for all conditions.

3.2. Second solidification condition

In order to observe only the influence of the solution time with two different microstructures, experiments were performed with two different cooling conditions using sand and metallic molds. Each condition was carried out twice. The as-solidified samples were extracted from the castings and subjected to solution heat treatment. The adopted nomenclature was: 2–1 – solution time about 8 h in both conditions (sand mold and chill mold); 2–2 – solution time about 12 h in both conditions; 2–3 – solution time about 16 h in the second condition (chill mold); 2–4 - solution time about 28 h in the second condition (chill mold).

3.2.1. Microstructures

The results of average secondary dendrite arm spacings obtained for two conditions in the four experiments are summarized in Table 3. The secondary dendrite arm spacings were related to the type of mold, sand and metallic, and consequently to the cooling rate, lower and higher respectively.

Fig. 13 shows examples of microstructures for the two conditions, where it is possible to note the presence of microporosity in interdendritic regions.

After the solution heat treatments, the samples were analyzed by optical microscopy in order to verify the dissolution of $CuAl_2$ particles. Fig. 14 presents metallographic images for aging times of 8, 12 and 28 h for samples solidified in the chill mold. As can be seen in Fig. 14, in the higher magnification images the dissolu-

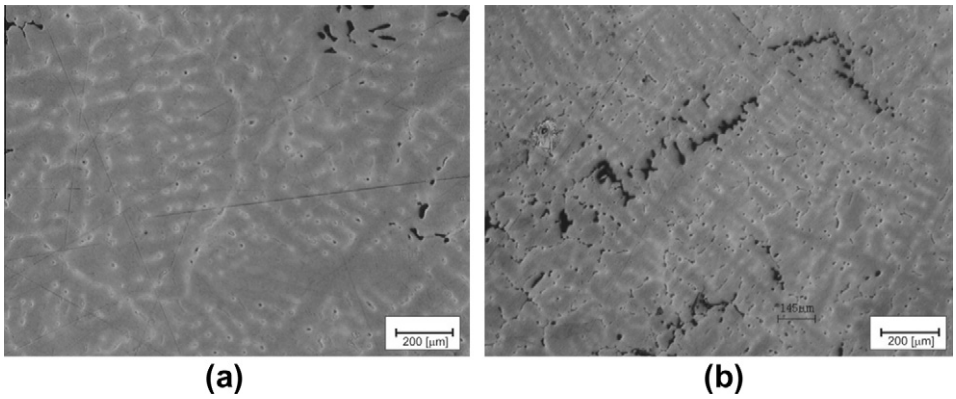

Fig. 13. As-cast metallographic images: (a) sand mold; (b) chill mold.

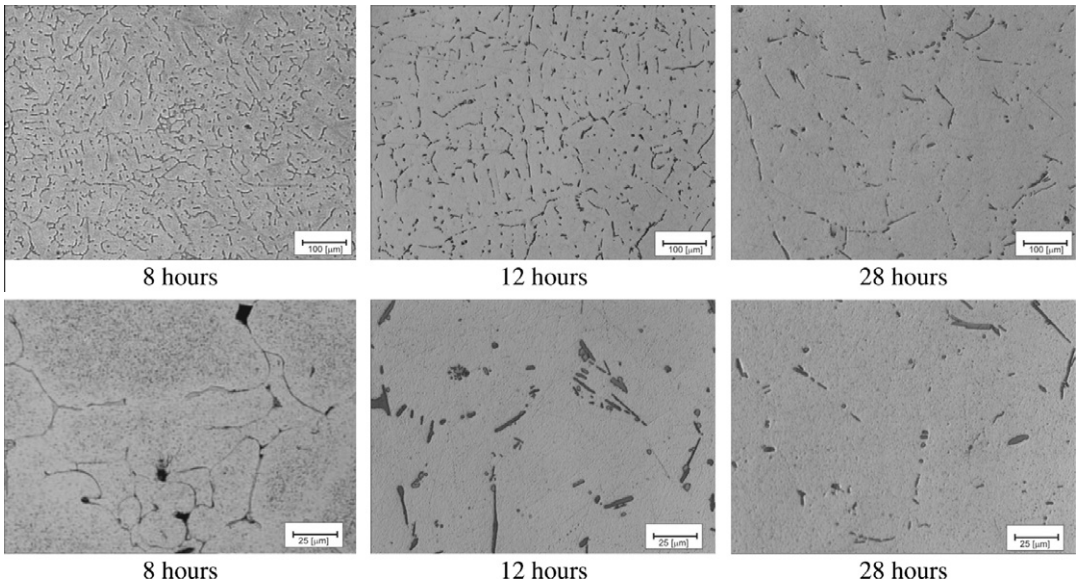

Fig. 14. Metallographic images of solution heat treated samples: chill mold (8, 12 and 28 h).

Table 4
Average Brinell hardness during natural aging for the second solidification condition.

Samples	As-cast	Solution heat treated	17 days	34 days	55 days	90 days
Sand–8 h	57.7	57.2	61.6	63.4	61.7	62.2
Sand–12 h	58.6	61.9	62.8	63.4	66.6	67.3
Chill–8 h	59.3	57.5	68.0	71.0	72.0	73.1
Chill–12 h	58.4	63.2	69.3	70.0	73.0	73.9
Chill–16 h	59.1	63.5	68.4	69.7	71.9	73.6
Chill–28 h	59.2	63.5	67.1	69.1	70.2	72.8

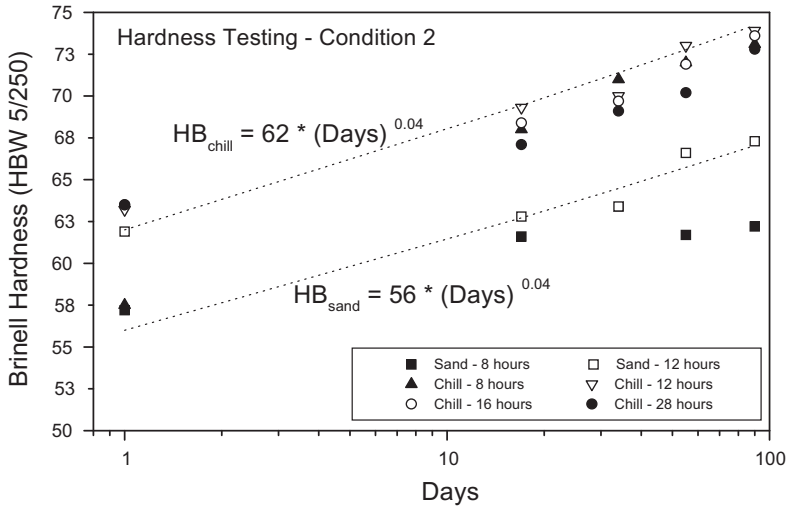

Fig. 15. Hardness as a function of solidification conditions, solution heat treated and naturally aged.

tion of $CuAl_2$ particles increases with the increase in solution time. However, some colonies of precipitates can still be observed up to an aging time of about 28 h. The results showed that for solution times less than 12 h, the network of continuous precipitates are not eliminated. A solution time of about 12 h seems to be the best condition for the solution heat treatment, since solution times >12 h did not give evidence of any significant difference.

The presence of microporosity in this solidification condition is caused by the pouring stage, which increases the turbulence and gas dragging. In the first condition, the casting is melted in situ and hence pouring is not necessary. This explains the small fraction of pores observed in the first solidification condition (about 0.5%) and a higher quantity in the second condition (about 6%). These values were determined in each specific position of the thermocouples, by subjecting the corresponding transverse microstructures to an image analyzer software.

3.2.2. Hardness testing

During aging, the precipitation hardening was also analyzed by Brinell hardness measurements, and the results are presented in the Table 4 and Fig. 15.

In the present study, the estimated error expected in temperature measurements is about 5% for the used thermocouples, and the accuracy of Brinell hardness is of two points on the scale. However, with a view to minimizing errors, all experiments were carried out twice and all measurements were made at least six times for each selected region.

4. Conclusions

The following major conclusions can be drawn from the present study:

- The hardness decreases with the increase in the secondary dendritic arm spacing, λ_2, for all conditions experimentally examined. Experimental laws correlating λ_2 with the solidification cooling rate and the Brinell hardness with λ_2 are proposed for unidirectional samples in the as-cast condition.
- A solution time of about 12 h was shown to be the best condition for the solution heat treatment since solution times higher than 12 h did not give evidence of any significant difference.
- Experimental equations are proposed relating the aging time with the resulting Brinell hardness for different solidification conditions: air cooled unidirectional solidification and multidirectional solidification in chill and sand molds.

Acknowledgements

The authors acknowledge the financial support provided by CNPq (The Brazilian Research Council), FAPERGS (The Scientific Research Foundation of the State of Rio Grande do Sul) and PUCRS (Pontifical Catholic University of Rio Grande do Sul).

References

[1] J.M.V. Quaresma, C.A. Santos, A. Garcia, Metal. Mat. Trans. A – Phys. Metal. Mat. Sci. 31A (2000) 1–14.
[2] W.R.R. Osório, C.A. Santos, J.M.V. Quaresma, A. Garcia, J. Mat. Proc. Technol. 6938 (2003) 1–7.
[3] W.R.R. Osório, J.E. Spinelli, N. Cheung, Mater. Sci. Eng. A 420 (2006) 179–186.
[4] P.R. Goulart, J.E. Spinelli, W.R.R. Osório, Mater. Sci. Eng. A 421 (2006) 245–253.
[5] P.R. Goulart, J.E. Spinelli, N. Cheung, Mater. Chem. Phys. 119 (2010) 272–278.
[6] M.V. Canté, J.E. Spinelli, N. Cheung, A. Garcia, Met. Mater. Int. 16 (2010) 39–49.
[7] K.S. Cruz, E.S. Meza, F.A.P. Fernandes, J.M.V. Quaresma, L.C. Casteletti, A. Garcia, Metal. Mat. Trans. A – Phys. Metal. Mat. Sci. 41A (2010) 972–984.
[8] B. Silva, I. Araujo, W. Silva, P.R. Goulart, A. Garcia, J.E. Spinelli, Philos. Mag. Lett. (Print) 91 (2011) 337–343.

[9] J.E. Spinelli, .N. Cheung, P.R. Goulart, J.M.V. Quaresma, A. Garcia, Int. J. Therm. Sci. 51 (2012) 145–154.
[10] L. Lasa, J.M. Rodriguez-Ibabe, J. Mater. Sci. 40 – 4 (2004) 1343–1355.
[11] M. Gavgali, B. Aksakal, Mater. Sci. Eng. A 254 (1998) 189–199.
[12] M.N. Grazyna, J. Sieniawski, J. Mat. Proc. Technol. 162–163 (2005) 367–372.
[13] E.J. Zoqui, M.H. Robert, J. Mat. Proc. Technol. 78 (1998) 198–203.
[14] ASM Handbook, Alloy Phase Diagrams, vol. 3, ASM International, 1992.
[15] B.P. Reis, Influence of as-cast structure in the solutioning conditions of the Al-4.0 wt% Cu alloy, Master Thesis, Graduation Program in Materials Engineering and Technology, Pontifical Catholic University of Rio Grande do Sul, 2009.
[16] E.M. Costa, C.E. Costa, F. Dalla Vecchia, C. Rick, M. Scherer, C.A.Santos, B.A. Dedavid, J. Alloys Comp. 488 (2010) 89–99.
[17] A. Schievenbush, G. Zimmermann, M. Matheus, Mater. Sci. Eng. A 173 (1993) 85–88.
[18] ASTM E 10-01, Standard Test Method for Brinell Hardness of Metallic Materials, Annual Book of ASTM Standards, vol. 03.01, 2004, pp. 1–9.
[19] M.L.M. Melo, C.L. Penhalber, N.A. Pereira, C.L. Pellicari Jr., C.A. Santos, J. Mater. Sci. 42 (2007) 2267–2275.
[20] M.L.M. Melo, E.M.S. Rizzo, R.G. Santos, J. Mater. Sci. 40–7 (2005) 1599–1609.